Antarctic Science page 1 of 12 *(2017)* © Antarctic Science Ltd 2017 doi:10.1017/S0954102016000602

NeQuick2 and IRI2012 models applied to mid and high latitudes, and the Antarctic ionosphere

M. PIETRELLA[1], B. NAVA[2], M. PEZZOPANE[1], Y. MIGOYA ORUE[2], A. IPPOLITO[1] and C. SCOTTO[1]

[1]*Istituto Nazionale di Geofisica e Vulcanologia, via di Vigna Murata 605, 00143 Rome, Italy*
[2]*The Abdus Salam International Centre for Theoretical Physics Strada Costiera 11, I-34051 Trieste, Italy*
marco.pietrella@ingv.it

Abstract: Within the framework of the AUSPICIO (AUtomatic Scaling of Polar Ionograms and Co-operative Ionospheric Observations) project, a limited sample of ionograms recorded mostly in 2001 and 2009, and to a lesser extent in 2006–07 and 2012–15, at the ionospheric observatories of Hobart and Macquarie Island (mid-latitude), Comandante Ferraz and Livingstone Island (high latitude), and Casey, Mawson, Davis and Scott Base (inside the Antarctic Polar Circle (APC)) were considered to study the capability of the NeQuick2 and IRI2012 models for predicting the behaviour of the ionosphere at mid- and high latitudes and over the Antarctic area. The applicability of NeQuick2 and IRI2012 was evaluated as i) climatological models taking as input the $F_{10.7}$ solar activity index and ii) assimilative models ingesting the *fo*F2 and *hm*F2 measurements obtained from the electron density profiles provided by the Adaptive Ionospheric Profiler (AIP). The statistical analysis results reveal that the best description of the ionosphere's electron density is achieved when the AIP measurements are ingested into the NeQuick2 and IRI2012 models. Moreover, NeQuick2 performance is far better than IRI2012 performance outside the APC. Conversely, the IRI2012 model performs better than the NeQuick2 model inside the APC.

Received 21 April 2016, accepted 15 October 2016

Key words: adaptive ionospheric profiler, autoscala, data ingestion, root mean square error

Introduction

Long-term prediction models developed in the past on the basis of monthly median measurements recorded at various ionospheric observatories are able to provide such reliable climatological predictions of the main ionospheric parameters that they do not require further improvements today. Some of them are regional (Hanbaba 1999 and references therein) others, such as the International Reference Ionosphere (IRI; Bilitza & Reinisch 2008, Bilitza 2015) and the NeQuick2 (Nava *et al*. 2008 and references therein), are global.

The importance of short-term forecasting models (Stanislawska & Zbyszynski 2002, Pietrella & Perrone 2008, Pietrella 2012, 2014), providing predictions for a few hours ahead, as well as nowcasting models (Araujo-Pradere *et al*. 2002, Zolesi *et al*. 2004, Pietrella & Perrone 2005) that provide real-time predictions, has also been acknowledged by the scientific community, especially in cases of a very disturbed ionosphere when the long-term models are unable to provide reliable forecasts.

The challenge today is the achievement of a comprehensive real-time 3-D specification of the ionosphere (nowcasting). In recent years, the increasing number of digisondes equipped with software that provides automatic real-time scaling of the main ionospheric parameters (Reinisch & Huang 1983, Pezzopane & Scotto 2007) has made it possible to develop nowcasting models the need of which is well recognized. To this regard a large number of models that ingest real-time data and then provide an

Table I. List of stations involved and their geographical co-ordinates.

Label	Station	Latitude	Longitude	Type of ionosonde	Scientific communities
1	Hobart	42°2'S	147°3'E	CADI	Ionospheric Prediction Service (Australia)
2	Macquarie Island	54°5'S	159°0'E	CADI	Ionospheric Prediction Service (Australia)
3	Comandante Ferraz	62°1'S	301°6'E	CADI	Istituto Nacional de Pesquisas Espaciais (Brazil)
4	Livingstone Island	62°7'S	299°6'E	AIS-INGV	Universitat Ramon Lull (Spain)
5	Casey[a]	66°3'S	110°5'E	CADI	Ionospheric Prediction Service (Australia)
6	Mawson[a]	67°6'S	62°9'E	IPS 42	Ionospheric Prediction Service (Australia)
7	Davis[a]	68°6'S	78°0'E	DIGISONDE	Ionospheric Prediction Service (Australia)
8	Scott Base[a]	77°8'S	166°8'E	IPS 42	Ionospheric Prediction Service (Australia)

[a]Located inside the Antarctic Polar Circle.

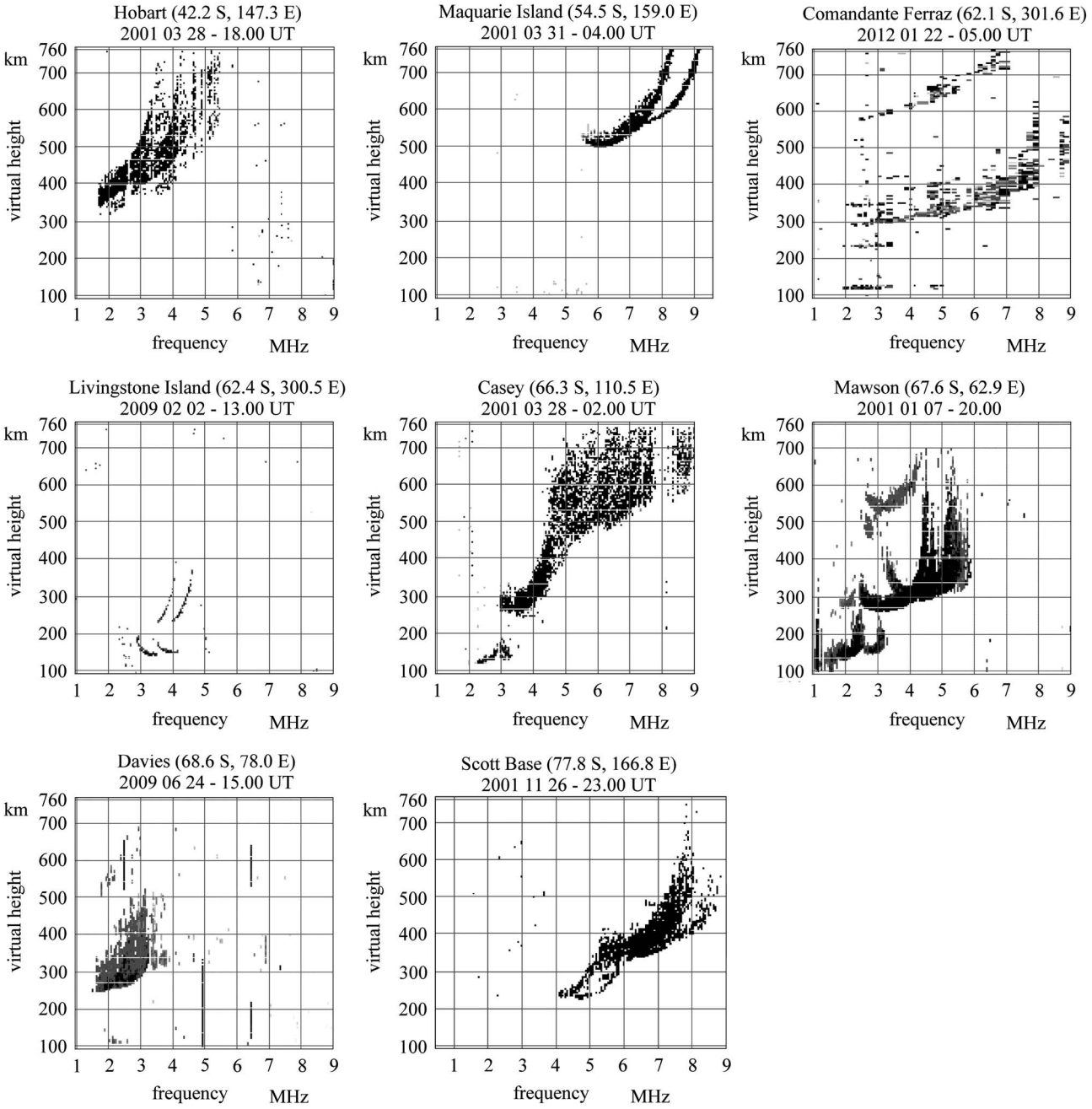

Fig. 1. Some examples of ionograms for which the Adaptive Ionospheric Profiler (AIP) cannot provide reliable *Ne*(*h*), recorded at **a.** Hobart (Hob), **b.** Macquarie Island (Mac Isl), **c.** Comandante Ferraz (Com Ferraz), **d.** Livingstone Island (Liv Isl), **e.** Casey (Cas), **f.** Mawson (Maw), **g.** Davis (Dav) and **h.** Scott Base (Scb).

updated 3-D mapping of the ionosphere has recently proposed (Galkin *et al.* 2012, Pezzopane *et al.* 2013).

The dataset considered in this study comprises a limited sample of ionograms which were provided within the framework of the Automatic Scaling of Polar Ionograms and Co-operative Ionospheric Observations (AUSPICIO) project and recorded principally in 2001 and 2009, and to a lesser extent in 2006–07 and 2012–15. Different epochs relative to these years, characterized by quiet and disturbed geomagnetic conditions, were selected and analysed during the winter and summer.

The ionograms under consideration were recorded by different types of ionosondes including the Digital Portable Sounder DPS-4 (Haines & Reinisch 1995), the IPS 42 (Titheridge 1993), the AIS-INGV (Zuccheretti *et al.* 2003) and the Canadian Advanced Digital Ionosonde (CADI; McDougall 1997). Table I summarizes the

Table II. Epochs analysed in the AUSPICIO project for each station. Bold indicates geomagnetically disturbed periods ($\sum K_p > 24$). Italic indicates quiet periods ($\sum K_p \leq 24$). The number of days for each period are in brackets. The total number of days (D_{TOT}) analysed for each station is also indicated in the bottom row.

Year	Dates	Hobart	Macquarie Island	Comandante Ferraz	Livingstone Island	Casey[a]	Mawson[a]	Davis[a]	Scott Base[a]
2001	*7–13 Jan*	x (7)					x (7)		
2001	*7–11, 13 Jan*		x 5)						
2001	**27–31 Mar, 1–2 April**	x (7)	x (7)			x (7)	x (7)		
2001	*28–30 Jun, 1–4 Jul*	x (7)	x (7)			x (7)			
2001	*25–30 Nov*								x (6)
2001	*21–25 Dec*								x (5)
2006	**26 Jan, 21 Feb**				x (2)				
2006	*6 Feb*				x (1)				
2007	**29, 31 Jan**				x (2)				
2009	*12, 18, 20, 22, 23 Jan, 2, 6 Feb*				x (7)				
2009	**4–5 Feb**	x (2)	x (2)			x (2)			x (2)
2009	**4 Feb**						x (1)		
2009	**22–23 Jul**		x (2)			x (2)	x (2)	x (2)	x (2)
2009	*30 Nov, 6 Dec*							x (7)	
2009	*7–13 Jan*	x (7)	x (7)			x (7)	x (7)		x (7)
2009	*24–25 Jun*		x (2)			x (2)	x (2)	x (2)	x (2)
2012	*18–21 Jan, 23–26 Jan*			x (8)					
2012	**22 Jan**			x (1)	x (1)				
2012	**12 Dec**				x (1)				
2013	*5, 11, 12, 14 Jan*				x (3)				
2014	*4, 5, 8, 13 Feb, 17 Dec*				x (5)				
2015	*4, 26 Jan*				x (2)				
2015	**7 Jan**				x (1)				
D_{TOT}		(30)	(32)	(9)	(25)	(27)	(26)	(11)	(24)

[a]Located inside the Antarctic Polar Circle.

ionospheric observatories, the types of ionosonde and the scientific communities involved in providing data.

The aim of this work is to assess the performance of the IRI2012 and NeQuick2 models, mainly at high latitudes and inside the Antarctic Polar Circle (APC). However, considering that the Australian Ionospheric Prediction Service also made data available from the mid-latitude stations of Hobart and Macquarie Island, the opportunity was taken to also investigate the behaviour of the models at these stations. Therefore, the ionograms considered in this study were recorded at the ionospheric observatories of Hobart and Macquarie Island (mid-latitude), Comandante Ferraz and Livingstone Island (high latitude), and Casey, Mawson, Davis and Scott Base (APC).

Table III. The theoretical and real ionograms database for each ionospheric observatory is shown in the first column. The subset of ionograms actually employed to carry out the statistical analyses with their corresponding percentages are also shown.

Label	Station	Theoretical number of AIP *Ne*(*h*)/ Real number of AIP *Ne*(*h*)	Number of selected AIP *Ne*(*h*)	Percentage
1	Hobart	720/720	69	10%
2	Macquarie Island	768/771	78	10%
3	Comandante Ferraz	216/216	89	45%
4	Livingstone Island	600/613	138	23%
5	Casey[a]	648/647	19	3%
6	Mawson[a]	624/587	33	6%
7	Davis[a]	264/264	13	5%
8	Scott Base[a]	576/557	5	≈ 1%

[a]Located inside the Antarctic Polar Circle.
AIP = Adaptive Ionospheric Profiler.

The Autoscala software, dedicated to the automatic scaling of ionograms (Scotto & Pezzopane 2002, Scotto 2009), was run on the ionograms recorded at the above-mentioned ionospheric observatories. Specifically, the Adaptive Ionospheric Profiler (AIP), which is an integral part of Autoscala, was applied to extract from each ionogram a real-time autoscaled electron density profile, *Ne*(*h*), which, in this study, is assumed to be the measured *Ne*(*h*); hereafter also referred to as the reference *Ne*(*h*) or simply the AIP profile.

Before starting evaluation of the performance of IRI2012 and NeQuick2, a preliminary check was carried out for each observatory to exclude any profiles provided by the AIP routine that were considered unreliable, and those retained were then selected and used as reference profiles.

This was necessary due to the complexity of the structure and dynamics of the high latitude ionosphere, which often gives rise to ionograms that are more diverse and difficult to interpret and autoscale than those recorded at mid-latitudes.

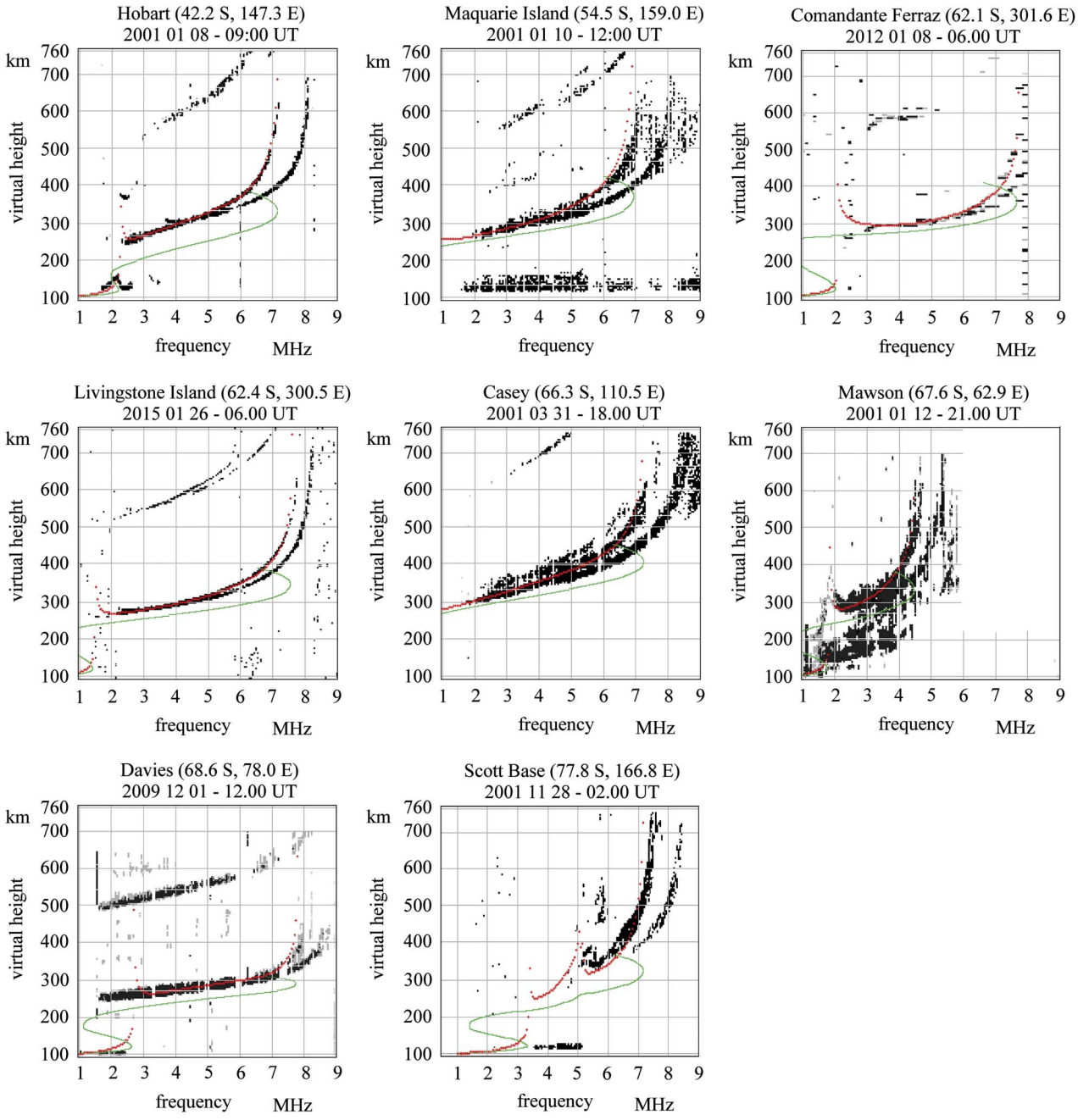

Fig. 2. Some examples of ionograms recorded at **a.** Hobart (Hob), **b.** Macquarie Island (Mac Isl), **c.** Comandante Ferraz (Com Ferraz), **d.** Livingstone Island (Liv Isl), **e.** Casey (Cas), **f.** Mawson (Maw), **g.** Davis (Dav) and **h.** Scott Base (Scb), along with the corresponding *Ne*(*h*) output by Adaptive Ionospheric Profiler (AIP; green traces) and ionograms reconstructed from the AIP profile (red traces), shown for different epochs.

This subject is discussed in more detail later in this paper. In these cases, the AIP does not succeed in providing a reliable *Ne*(*h*). Some examples of ionograms from which the AIP is not able to provide a reference *Ne*(*h*) are presented in Fig. 1.

The selected AIP profiles (some examples of which are also shown in Fig. 2) were compared with: i) the *Ne*(*h*) output by the climatological models NeQuick2 and IRI2012, taking as input the $F_{10.7}$ solar activity index and ii) the *Ne*(*h*) provided by the NeQuick2 and IRI2012 models when used as assimilative models, ingesting the values of the critical frequency of the F2 layer (*fo*F2) and the maximum height of the F2 layer (*hm*F2) obtained automatically in the ionogram inversion procedure used by Autoscala, which is fully discussed by Scotto (2009).

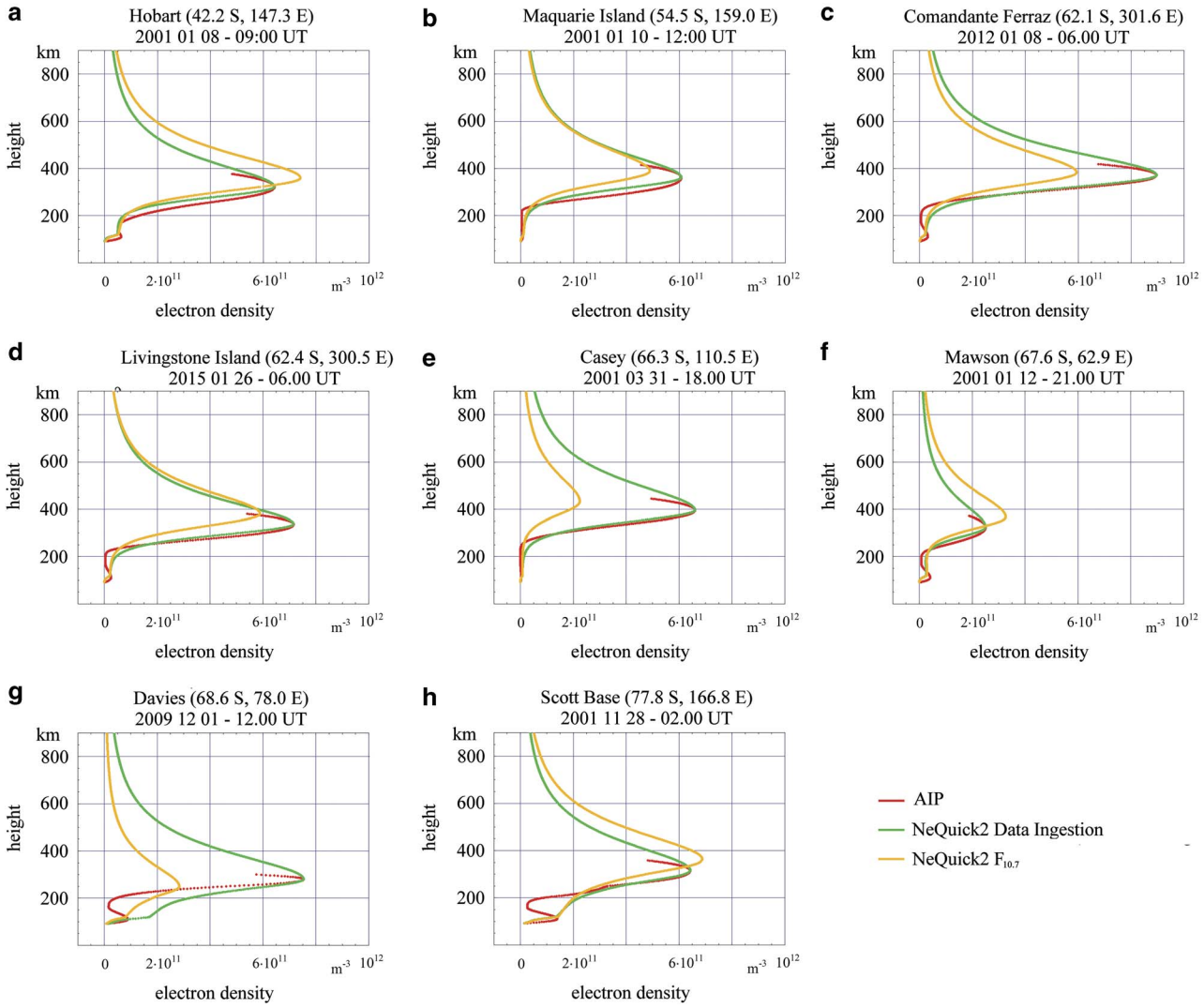

Fig. 3. Some examples of comparisons between the Adaptive Ionospheric Profiler (AIP) *Ne*(*h*) (red plot) and NeQuick2 *Ne*(*h*) generated by ingesting bottomside parameters (green plot) and in long-term (yellow plot) prediction mode at **a.** Hobart (HOB), **b.** Macquarie Island (MAC), **c.** Comandante Ferraz (C. FER), **d.** Livingstone Island (LIV), **e.** Casey (CAS), **f.** Mawson (MAW), **g.** Davis (DAV) and **h.** Scott Base (SCB), shown for the same epochs and ionospheric observatories as the ionograms depicted in Fig. 2.

To include cases characterized by disturbed magnetic/ionospheric conditions, IRI2012 was employed with the STORM option set to 'ON'. Some example comparisons between the AIP profiles and the NeQuick2 and IRI2012 *Ne*(*h*) in both long-term and real-time prediction mode are also shown. The comparisons between NeQuick2 and IRI2012 performance, evaluated in terms of root mean square error (r.m.s.e.), are shown for each ionospheric observatory.

Data ingestion technique

The technique allowing the ingestion of the F2 ionosphere layer parameters, i.e. *fo*F2 and *hm*F2 deduced from ionosonde measurements, into the NeQuick2 ionosphere electron density model has repeatedly proven to be very effective for providing highly comprehensive specification of the ionosphere (Buresova *et al*. 2009, Nava *et al*. 2011).

The NeQuick2 adaptation to ionosonde-derived peak values is based on the use of effective parameters. Considering the ITU-R coefficients and the relevant gamma functions implemented in the NeQuick2 model, which serve to compute the critical frequency of the F2 layer, *Az_fo*F2 was defined as the effective $F_{10.7}$ value that allows NeQuick2 to match the *fo*F2 value measured at a given reference ionospheric observatory (Buresova *et al*. 2009).

In a similar way, by means of the Dudeney formula for *hm*F2 implemented in the NeQuick2 model, *Az_hm*F2 was defined as the effective $F_{10.7}$ value that allows NeQuick2 to match the experimental *hm*F2 value at the

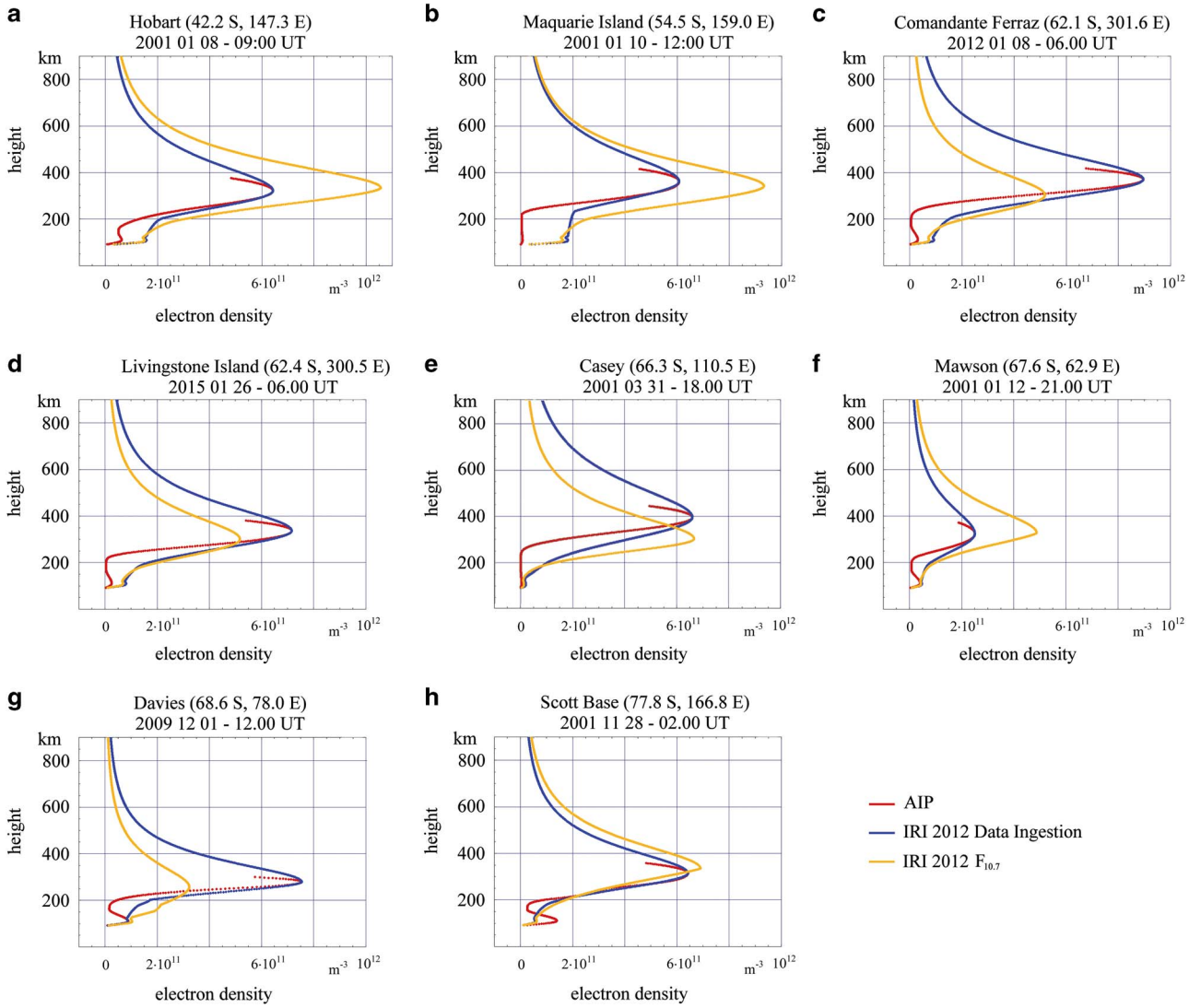

Fig. 4. Some examples of comparisons between the Adaptive Ionospheric Profiler (AIP) *Ne*(*h*) (red plot) and IRI2012 *Ne*(*h*) generated by ingesting bottomside parameters (green plot) and in long-term (yellow plot) prediction mode at **a.** Hobart (HOB), **b.** Macquarie Island (MAC), **c.** Comandante Ferraz (C. FER), **d.** Livingstone Island (LIV), **e.** Casey (CAS), **f.** Mawson (MAW), **g.** Davis (DAV) and **h.** Scott Base (SCB), shown for the same epochs and ionospheric observatories as the ionograms depicted in Fig. 2.

reference ionospheric observatory under consideration. Once these effective parameters have been calculated, they can also be used to estimate *fo*F2 and *hm*F2 values over the region surrounding the reference station (Nava *et al.* 2011).

IRI2012 *Ne*(*h*) were obtained by applying a data ingestion method conceptually similar to the one described for the NeQuick2 model. Using the ingestion technique mentioned above, the differences between the modelled *hm*F2 and the ones obtained at different ionosonde stations were minimized within a certain tolerance. The inferred-IG values thus obtained can be used to generate a 3-D representation of the ionosphere (Migoya-Oruè *et al.* 2015), and retrieve the full *Ne*(*h*) with IRI2012, as in this study.

In the present work, the *fo*F2 and *hm*F2 measurements ingested into the IRI2012 and NeQuick2 models were those provided automatically by Autoscala (Scotto 2009).

Results

Due to the complexity of the high latitude ionosphere structure, the ionograms recorded at the ionospheric observatories listed in Table I are often characterized by extensive spread-F phenomena and z-ray traces, making the automatic scaling procedure very difficult. For this reason, a preliminary study was conducted on each ionospheric observatory to exclude cases in which the

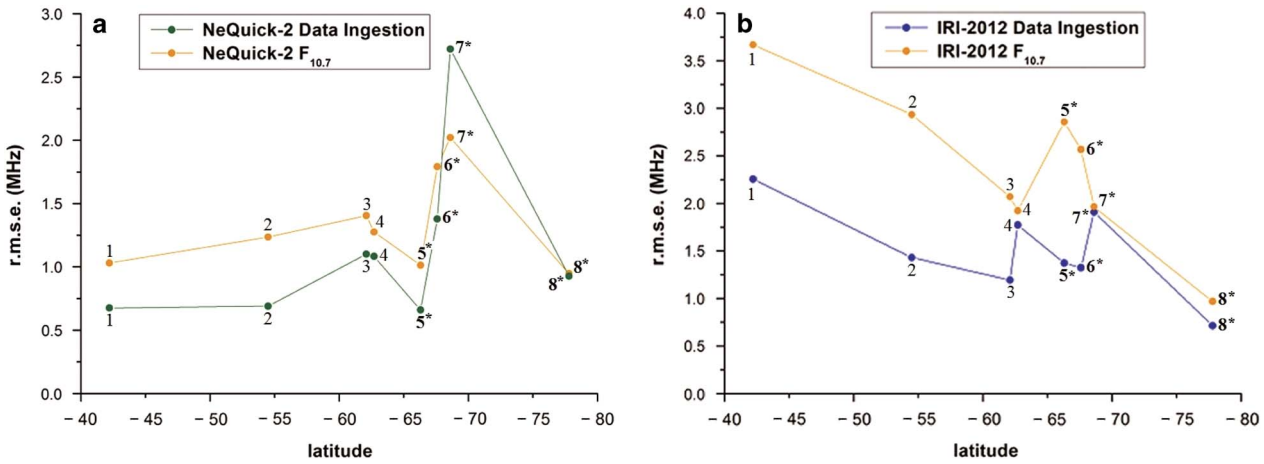

Fig. 5. Root mean square error (r.m.s.e.) for each station, as labelled in Table I, by **a.** the NeQuick2 Data Ingestion (green dots) and NeQuick2 $F_{10.7}$ (yellow dots) models, **b.** the IRI2012 Data Ingestion (blue dots) and IRI2012 $F_{10.7}$ (yellow dots) models, as a function of geographical latitude. * marks the ionospheric observatories located inside the Antarctic Polar Circle.

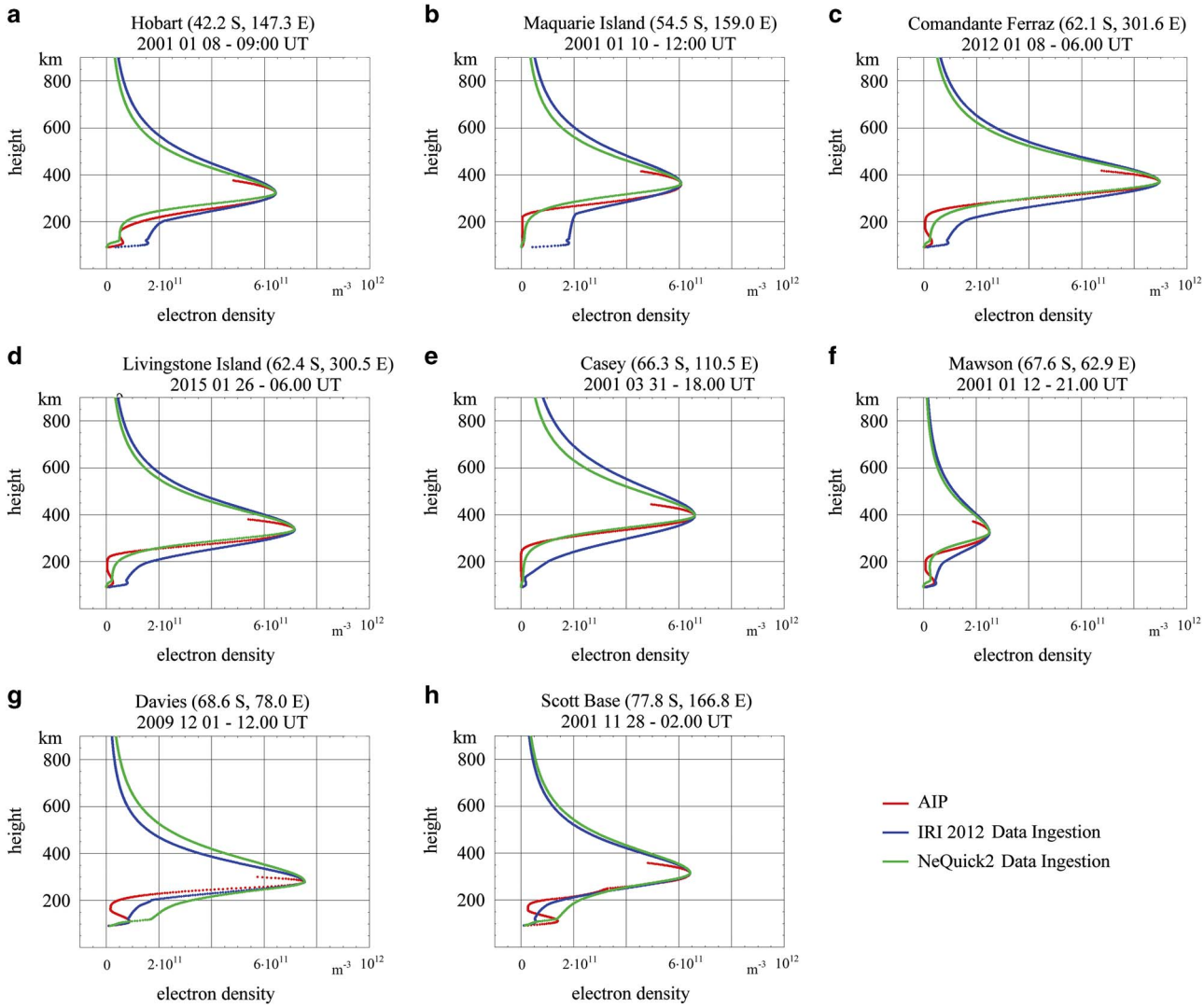

Fig. 6. As in Fig. 3, but for the IRI2012 and NeQuick2 Data Ingestion models.

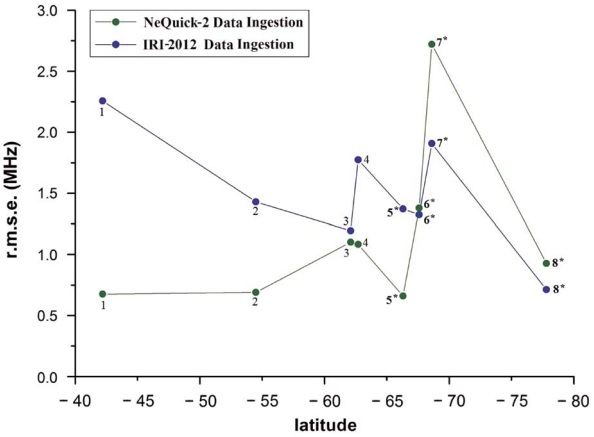

Fig. 7. Trend of root mean square error (r.m.s.e.) obtained by the NeQuick2 Data Ingestion (green dots) and IRI2012 Data Ingestion (blue dots) models as a function of geographical latitude. * marks the ionospheric observatories located inside the Antarctic Polar Circle.

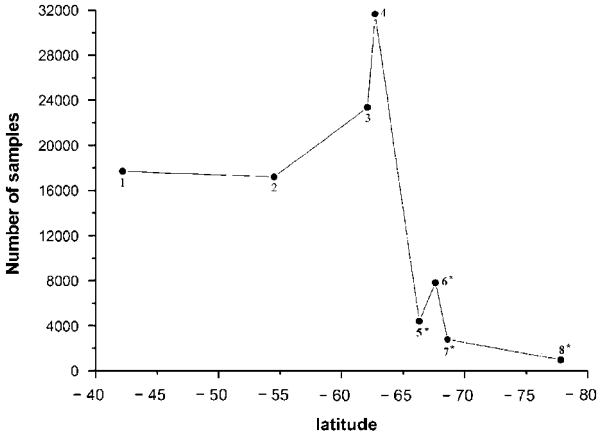

Fig. 8. Number of samples as a function of geographical latitude. * marks the ionospheric observatories located inside the Antarctic Polar Circle.

AIP failed to provide reliable *Ne*(*h*), selecting only the AIP profiles considered reliable and hence adopted as references. Several AIP *Ne*(*h*) were rejected as a consequence of this preliminary study and some examples of ionograms for which the AIP routine cannot provide *Ne*(*h*) are shown in Fig. 1.

The ionograms database to which the AIP was applied mainly refers to 2001 and 2009. For these years, a limited sample of ionograms recorded in both the winter and summer, as far as possible simultaneously available in all the stations, was considered for some quiet and geomagnetically disturbed epochs: 27–31 March, 1–2 April, 28–30 June and 1–4 July for 2001, 7–13 January, 4–5 February, 24–25 June and 22–23 July for 2009. In addition, a limited sample of ionograms from 2006–07 and 2012–15 were also considered, essentially to extend the analysis over the stations of Comandante Ferraz and Livingstone Island, which are only operative during summer. Table II shows the periods analysed in this study for each station in more detail.

The ionograms are recorded at a sampling rate of 60 min at each station, and so the theoretical number of ionograms to be considered for the analysis is given by the total number of days (D_{TOT}) shown in Table II multiplied by 24. However, the sampling rate sometimes sporadically changes to 30 min, with the result that the real number of *Ne*(*h*) analysed can be greater than the theoretical number, and vice versa, because ionosonde observations are occasionally missing and the real number of *Ne*(*h*) analysed is less than the theoretical number.

Table III summarizes the theoretical number of AIP *Ne*(*h*) for each ionospheric observatory, the real number of AIP *Ne*(*h*) analysed, and the number of AIP *Ne*(*h*) actually selected and then used as reference profiles.

It is important to point out that the selected AIP *Ne*(*h*) are 'validated' data in the sense that they are derived from 'validated' ionograms, i.e. from ionograms for which the values of *fo*F2 and *hm*F2 obtained manually by an operator match those given by Autoscala, and for which the restored trace starting from the obtained *Ne*(*h*) matches the recorded trace. Some examples of AIP *Ne*(*h*) along with the corresponding ionograms from which the AIP profiles were derived are shown in Fig. 2.

For each ionospheric observatory, the selected AIP profiles were compared with the *Ne*(*h*) provided by NeQuick2 operating under two different modes: i) as a climatological model taking as input the $F_{10.7}$ solar activity index (hereafter, NeQuick2 $F_{10.7}$) and ii) as an assimilative model ingesting the *fo*F2 and *hm*F2 measurements obtained from the *Ne*(*h*) provided by the AIP (hereafter, NeQuick2 Data Ingestion or NQ-DI). Some examples of these comparisons are shown in Fig. 3.

For each ionospheric observatory, the selected AIP profiles were also compared to the *Ne*(*h*) provided by the climatological IRI2012 model (hereafter, IRI2012 $F_{10.7}$) and the *Ne*(*h*) obtained from the assimilative IRI2012 model (hereafter, IRI2012 Data Ingestion or I-DI). Some examples of these comparisons are shown in Fig. 4.

A visual inspection of a very large number of comparisons, such as those shown in Figs 3 & 4, clearly reveals that the assimilation of autoscaled data, i.e. the *fo*F2 and *hm*F2 values, is crucially important for achieving more reliable ionospheric modelling.

As a preliminary step, for each ionospheric observatory the AIP profiles selected up to the bottomside and the corresponding *Ne*(*h*) modelled by the NQ-DI, NeQuick2 $F_{10.7}$, I-DI and IRI2012 $F_{10.7}$ were added up, in order to have a larger number of samples from which to calculate a statistically more significant r.m.s.e. From the

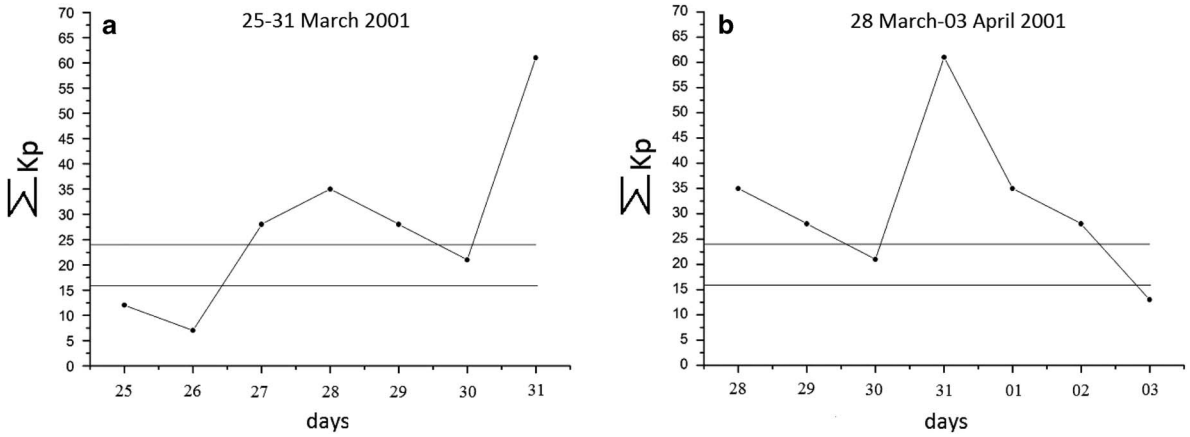

Fig. 9. Geomagnetic activity expressed in terms of $\sum K_p$ **a.** three days before and three days after 28 March 2001, the day of the ionograms recorded at Hobart at 18h00 UT and Casey at 02h00 UT, **b.** three days before and three days after 31 March 2001, the day of the ionogram recorded at Macquarie Island at 04h00 UT. The horizontal lines mark the levels of $\sum K_p = 16$, above which the occurrence frequency of large-scale gravity waves reaches 25/27 (Testud 1970), and $\sum K_p = 24$, below which magnetic conditions can be considered quiet.

five different databases thus obtained, the r.m.s.e. was calculated as follows:

$$rmse_{NQ\text{-}DI} = \sqrt{\frac{\sum_{h\min=91km}^{h\max=hmF2km} (fp(h)_{AIP} - fp(h)_{NQ\text{-}DI})^2}{N}}$$

$$rmse_{NeQuick\,2F10.7} = \sqrt{\frac{\sum_{h\min=91km}^{h\max=hmF2km} (fp(h)_{AIP} - fp(h)_{NeQuick2F10.7})^2}{N}}, \quad (1a)$$

$$rmse_{I\text{-}DI} = \sqrt{\frac{\sum_{h\min=91km}^{h\max=hmF2km} (fp(h)_{AIP} - fp(h)_{\text{I-DI}})^2}{N}}$$

$$rmse_{IRI2012F10.7} = \sqrt{\frac{\sum_{h\min=91km}^{h\max=hmF2km} (fp(h)_{AIP} - fp(h)_{IRI2012F10.7})^2}{N}}. \quad (1b)$$

In Eq. (1a) & (1b), N is the total number of samples ($fp(h)$ values), $fp(h)AIP$, is the reference plasma frequency given by AIP, $fp(h)NQ\text{-}DI$, $fp(h)NeQuick2F10.7$, $fp(h)I\text{-}DI$ and $fp(h)IRI2012F10.7$ are the plasma frequencies modelled respectively by NQ-DI, NeQuick2 $F_{10.7}$, I-DI and IRI2012 $F_{10.7}$ at a definite real height (h).

The r.m.s.e. analysis results are shown in Fig. 5 and demonstrate that the NQ-DI and I-DI models perform better than the NeQuick2 $F_{10.7}$ and IRI2012 $F_{10.7}$ models, respectively. Some examples of comparisons between the AIP, NQ-DI and I-DI $Ne(h)$ are shown in Fig. 6. To better highlight a possible dependence of performance on geographical latitude, a direct comparison between the r.m.s.e. values provided by NQ-DI and I-DI is also plotted in Fig. 7 as a function of the geographical latitude of the ionospheric observatories considered in this study. The number of samples on which the r.m.s.e. is calculated for each ionospheric observatory is also plotted as a function of geographical latitude and shown in Fig. 8. Starting from the APC, a marked decrease in the number of samples included in the statistical analysis is observed.

Discussion

A visual inspection of a very large number of comparisons between the $Ne(h)$ provided by NeQuick2 and IRI2012, when operating both as climatological and assimilative models, shows unequivocally that a better specification of the ionosphere is provided by the NQ-DI and I-DI models (see the examples in Fig. 3 for NeQuick2 and Fig. 4 for IRI2012). This is also quantitatively confirmed when comparing the r.m.s.e. values provided by IRI2012 and NeQuick2 before and after the ingestion of bottomside parameters; in fact, except for Davis (case NeQuick2), the r.m.s.e. are greater when the standard climatological models are considered (see Fig. 5).

This means that: i) the NeQuick2 and IRI2012 models less efficiently represent the real behaviour of the high latitude ionosphere when operating in long-term prediction mode and ii) the best description of the ionospheric environment at southern mid and high latitudes and over the Antarctic area is provided when autoscaled $foF2$ and $hmF2$ values are ingested into the NeQuick2 and IRI2012 models. These results again confirm how the data ingestion techniques already investigated in some previous studies (Nava *et al.* 2011, Pezzopane *et al.* 2011, 2013, Pietrella *et al.* 2016, Sabbagh *et al.* 2016) can provide better results than the climatological models.

The r.m.s.e. at Hobart, Macquarie Island, Comandante Ferraz, Livingstone Island and Casey produced by NQ-DI and I-DI are, respectively, 0.68 *vs*

2.26 MHz, 0.69 *vs* 1.43 MHz, 1.10 *vs* 1.20 MHz, 1.08 *vs* 1.77 MHz and 0.66 *vs* 1.37 MHz. This means that, up to the APC, including Casey which lies just over the APC, NQ-DI performs far better than I-DI, making r.m.s.e. much smaller than those produced by I-DI. The situation is different when considering the ionospheric observatories of Mawson, Davis and Scott Base, where the r.m.s.e. produced by NQ-DI and I-DI are, respectively, 1.38 *vs* 1.33 MHz, 2.72 *vs* 1.91 MHz and 0.93 *vs* 0.71 MHz. These results reveal that beyond the APC, I-DI performs better than NQ-DI, particularly at Davis and Scott Base, although in the latter case only a small number of available samples were considered.

It is important to note that these results were achieved for a relatively limited ionograms database and for this reason they should be considered as strictly preliminary. One reason for the scarcity of ionograms, as already mentioned, is the extreme complexity of the high latitude ionosphere. This is explained by the fact that, while at mid-latitudes, the main sources of ionization are ultra-violet (UV) and x-ray emissions from the Sun, at high latitudes the Earth's magnetic field is structured such that, when the north–south direction (Bz) of the interplanetary magnetic field is orientated southwards ($Bz < 0$), the geomagnetic field lines can connect to the outer magnetosphere. When this occurs, solar wind particles, mainly electrons and protons, come directly into the ionosphere and represent an additional source of ionization to the UV and x-rays, considerably complicating the structure of the high latitude ionosphere. The solar wind and the occurrence of a $Bz < 0$ thus play an important role in the dynamics and behaviour of the ionosphere at high latitudes, which can thus be characterized by magneto-ionospheric storms, auroral phenomena, 'troughs' of lower ionization at subauroral latitudes, polar cup patches and Sun-aligned arcs. All this makes the morphology of the high latitude ionosphere considerably more complicated and different in general from the morphology of the mid-latitude ionosphere. In particular, polar cup patches are manifested as localized regions of enhanced electron density on spatial scales ranging from 200 to 1000 km horizontally (Moskaleva & Zaalov 2013). Other large-scale structural features exhibiting augmented electron density include Sun-aligned arcs, characterized by a dusk–dawn drift (Hunsucker & Hargreaves 2003).

Electron density gradients related to these large-scale high latitude ionospheric inhomogeneities have an important effect on the propagation of high frequency (HF) radio signals. In fact, very large deviations on the direction of arrival of HF radio signals, with bearings up to $\pm 100°$, have been attributed to the trough at subauroral latitudes (Siddle *et al.* 2004a, 2004b), as well as to the presence of patches and arcs of enhanced electron density (Warrington *et al.* 1997). Moreover, as also observed at mid-latitudes, electron density inhomogeneities roughen the reflecting surface, increasing the directional spread of signals arriving at the receiver (Bianchi *et al.* 2013). The complexity of the structure and dynamics of the high latitude ionosphere is clearly reflected in ground-based observations based on vertical ionosonde soundings. Ionograms recorded at high latitudes are often rather different from those recorded at mid-latitudes. Due to scattering from large-scale ionospheric irregularities, radio echoes reflected from the F2 layer have a longer duration than the transmitted pulses, which can cause a relatively large spread of signals from the F2 layer, usually referred to as the spread-F phenomenon (Shimazaki 1962). Often the spread-F phenomenon is so widespread that it is very difficult, if not impossible, to determine the value of *fo*F2 from the ionogram.

Some examples of these ionograms are shown in Fig. 1. A careful analysis of the geomagnetic activity calculated in terms of $\sum K_p$ (where K_p is the three hourly magnetic planetary index and $\sum K_p$ its sum for one day, for download see http://wdc.kugi.kyoto-u.ac.jp/kp/index.html) revealed that the spread-F event observed in the ionograms recorded on 28 March 2001 at Hobart and Casey, and on 31 March 2001 at Macquarie Island, could be caused by ionospheric irregularities resulting from the presence of obliquely tilted iso-electron density surfaces caused by large-scale wave structures (LSWS) related to the propagation of gravity waves triggered by the geomagnetic activity.

The values for geomagnetic activity expressed in terms of $\sum K_p$, observed around 27–28 March (see Fig. 9a), are > 16, making them compatible with an LSWS occurrence frequency of 25/27 (Testud 1970). It is thus highly probable that these disturbed conditions triggered a LSWS, which was responsible for the spread-F phenomena observed at Hobart and Casey on 28 March 2001. On the other hand, the geomagnetic conditions observed in the time interval 28–31 March 2001 (see Fig. 9b), characterized by $\sum K_p$ values always > 16, could have triggered another LSWS and caused the spread-F phenomenon observed at Macquarie Island.

Another important feature of high latitude ionograms is the so-called z-ray (Bowman 1960). This consists of a third trace appearing on ionograms which, like spread-F, can lead to an uncertain determination of *fo*F2 (Scotto 2015). Moreover, the absorption suffered by the electromagnetic waves propagating into the D region, when this is strongly ionized by high energy protons emitted during solar flares (polar cup absorption (PCA) events), gives rise to blank ionograms, thus limiting the number of usable ionograms. Spread-F, z-ray and blank ionograms are therefore expressions of the considerably greater complexity and turbulence of high latitude ionosphere morphology compared to mid-latitudes. Consequently, the automatic recognition of resolved (possibility of routinely scaling *fo*F2

and *hm*F2) and unresolved (impossibility of routinely scaling *fo*F2 and *hm*F2 as in the example ionograms shown in Fig. 1) spread-F phenomena, along with the automatic recognition of z-ray (Scotto & Pezzopane 2012, Scotto 2015) and blank ionograms due to PCA events, constitute the most serious problems to resolve for any automatic scaling software (Reinisch & Huang 1983, Reinisch *et al*. 2005). Therefore, the number of reliable ionograms available for this study was greatly limited. This clearly emerges in Fig. 8, where a drastic decrease in the number of data involved in the statistical analysis is observed for the ionospheric observatories located inside the APC. This is directly due to the growing complexity of the ionosphere with increasing latitude for all the reasons described above.

Conclusions

Despite the genuine difficulty of autoscaling ionograms recorded at high latitudes, the authors are confident that by improving the capability of Autoscala to resolve spread-F and z-ray phenomena and reject bad quality ionograms (those that cannot even be scaled manually), while at the same time increasing the number of ionograms on which the AIP can operate, it would certainly be possible to obtain a larger number of reference profiles than those considered in the present investigation. This would enable more significant results from a statistical point of view, as well as a more detailed study on the applicability of NQ-DI and I-DI, exploring their prediction capacity under more diverse geophysical conditions. These studies could help establish which model is more suitable for application, which would be extremely valuable because it would also permit calculation of $Ne(h)$ over the regions surrounding the reference stations using the autoscaled values of *fo*F2 and *hm*F2.

It would be very worthwhile if these results could be achieved in the future, considering how the automatic scaling of vertical ionograms recorded at mid-latitudes has already proved effective in providing data for improved 3-D real-time specification of the ionosphere. Therefore, improvements for autoscaling ionograms recorded at high latitudes, to provide an ever-greater number of reliable $Ne(h)$, and the applicability of NQ-DI or I-DI in the above-mentioned sense, would represent an interesting approach for achieving nowcasting 3-D electron density mapping and, consequently, space weather forecasting in the ionospheric domain at high latitudes and in polar regions.

Acknowledgements

The authors would like to thank the following scientific institutions: the Ionospheric Prediction Service (Australia) for providing the ionograms database for Hobart, Macquarie Island, Casey, Mawson, Davis and Scott Base, the Istituto Nacional de Pesquisas Espaciais (Brazil) for providing the ionograms for Comandante Ferraz, the Universitat Ramon Lull (Spain) for providing the ionograms for Livingstone Island, and the Progetto Nazionale Ricerche in Antartide for supporting this study. The authors are very grateful to the anonymous referees for their useful comments and suggestions which have greatly contributed to improve the paper.

Author contributions

Marco Pietrella carried out the preliminary study aimed at selecting only the AIP electron density profiles considered to be reliable, he then rearranged the results provided by the other authors and drafted the manuscript. Bruno Nava suitably modified the NeQuick2 model to run as both a climatological and assimilative model, providing comparisons with the AIP electron density profiles. Michael Pezzopane converted the raw ionograms provided by the CADI ionosonde into the RDF format, which is ingested by Autoscala. Yenca Migoya Oruè suitably modified the IRI2012 model to run as both a climatological and assimilative model, providing comparisons with the AIP electron density profiles. Alessandro Ippolito and Carlo Scotto participated in the selection of the AIP electron density profiles, converted ionograms in different formats into the RDF format and adjusted Autoscala for the different ionospheric stations. All the authors actively participated in the discussion of the results and validation of the electron density profiles, as well as reading and approving the final manuscript.

References

Araujo-Pradere, E.A., Fuller-Rowell, T.J. & Codrescu, M.V. 2002. STORM: an empirical storm-time ionospheric correction model. 1. Model description. *Radio Science*, **37**, 10.1029/2001RS002467.

Bianchi, C., Baskaradas, J.A., Pezzopane, M., Pietrella, M., Sciacca, U. & Zuccheretti, E. 2013. Fading in the HF channel and role of irregularities. *Advances in Space Research*, **52**, 10.1016/j.asr.2013.03.035.

Bilitza, D. 2015. The international reference ionosphere – status 2013. *Advances in Space Research*, **55**, 10.1016/j.asr.2014.07.032.

Bilitza, D. & Reinisch, B.W. 2008. International reference ionosphere 2007: improvements and new parameters. *Advances in Space Research*, **42**, 10.1016/j.asr.2007.07.048.

Bowman, G.G. 1960. Triple splitting with the F2-region of the ionosphere at high and mid-latitudes. *Planetary and Space Science*, **2**, 10.1016/0032-0633(60)90018-0.

Buresova, D., Nava, B., Galkin, I., Angling, M., Stankov, S.M. & Coisson, P. 2009. Data ingestion and assimilation in ionospheric models. *Annals of Geophysics*, **52**, 235–253.

Galkin, I.A., Reinisch, B.W., Huang, X. & Bilitza, D. 2012. Assimilation of GIRO data into a real-time IRI. *Radio Science*, **47**, 10.1029/2011RS004952.

Haines, D.M. & Reinisch, B.W. 1995. *Digisonde portable sounder system manual*. Lowell, MA: University of Massachusetts Lowell Center for Atmospheric Research.

HANBABA, R. 1999. *Improved quality of services in ionospheric telecommunication systems planning and operation, Action 251, final report*. Warsaw: Space Research Center.

HUNSUCKER, R.D. & HARGREAVES, J.K. 2003. *The high-latitude ionosphere and its effects on radio propagation*. New York: Cambridge University Press, 617 pp.

MCDOUGALL, J.W. 1997. *Canadian advanced digital ionosonde user's manual*. London, ON: University of Western Ontario, Scientific Instrumentation.

MOSKALEVA, E.V. & ZAALOV, N.Y. 2013. Signature of polar cap inhomogeneities in vertical sounding data. *Radio Science*, **48**, 10.1002/rds.20060.

MIGOYA-ORUE, Y., NAVA, B., RADICELLA, S. & ALAZO-CUARTAS, K. 2015. GNSS derived TEC data ingestion into IRI 2012. *Advances in Space Research*, **55**, 10.1016/j.asr.2014.12.033.

NAVA, B., COISSON, P. & RADICELLA, S.M. 2008. A new version of the NeQuick ionosphere electron density model. *Journal of Atmospheric and Solar - Terrestrial Physics*, **70**, 10.1016/j.jastp.2008.01.015.

NAVA, B., RADICELLA, S.M. & AZPILICUETA, F. 2011. Data ingestion into NeQuick 2. *Radio Science*, **46**, 10.1029/2010RS004635.

PEZZOPANE, M. & SCOTTO, C. 2007. Automatic scaling of critical frequency *fo*F2 and *MUF*(*3000*)F2: a comparison between autoscala and ARTIST 4.5 on Rome data. *Radio Science*, **42**, 10.1029/2006RS003581.

PEZZOPANE, M., PIETRELLA, M., PIGNATELLI, A., ZOLESI, B. & CANDER, L.R. 2011. Assimilation of autoscaled data and regional and local ionospheric models as input sources for real-time 3-D International Reference Ionosphere modeling. *Radio Science*, **46**, 10.1029/2011RS004697.

PEZZOPANE, M., PIETRELLA, M., PIGNATELLI, A., ZOLESI, B. & CANDER, L.R. 2013. Testing the three-dimensional IRI-SIRMUP-P mapping of the ionosphere for disturbed periods. *Advances in Space Research*, **52**, 10.1016/j.asr.2012.11.028.

PIETRELLA, M. 2012. A short-term ionospheric forecasting empirical regional model (IFERM) to predict the critical frequency of the F2 layer during moderate, disturbed, and very disturbed geomagnetic conditions over the European area. *Annales Geophysicae*, **30**, 10.5194/angeo-30-343-2012.

PIETRELLA, M. 2014. Short-term forecasting regional model to predict *M*(*3000*)F2 over the European sector: comparisons with the IRI model during moderate, disturbed, and very disturbed geomagnetic conditions. *Advances in Space Research*, **54**, 10.1016/j.asr.2014.03.018.

PIETRELLA, M. & PERRONE, L. 2005. Instantaneous space-weighted ionospheric regional model for instantaneous mapping of the critical frequency of the F2 layer in the European region. *Radio Science*, **40**, 10.1029/2003RS003008.

PIETRELLA, M. & PERRONE, L. 2008. A local ionospheric model for forecasting the critical frequency of the F2 layer during disturbed geomagnetic and ionospheric conditions. *Annales Geophysicae*, **26**, 10.5194/angeo-26-323-2008.

PIETRELLA, M., PEZZOPANE, M. & SETTIMI, A. 2016. Ionospheric response under the influence of the solar eclipse occurred on 20 March 2015: importance of autoscaled data and their assimilation for obtaining a reliable modeling of the ionosphere. *Journal of Atmospheric and Solar - Terrestrial Physics*, **146**, 10.1016/j.jastp.2016.05.006.

REINISCH, B.W. & HUANG, X. 1983. Automatic calculation of electron density profiles from digital ionograms: 3. Processing of bottom side ionograms. *Radio Science*, **18**, 10.1029/RS018i003p00477.

REINISCH, B.W., HUANG, X., GALKIN, I.A., PAZNUKHOV, V. & KOZLOV, A. 2005. Recent advances in real-time analysis of ionograms and ionospheric drift measurements with digisondes. *Journal of Atmospheric and Solar - Terrestrial Physics*, **67**, 10.1016/j.jastp.2005.01.009.

SABBAGH, D., SCOTTO, C. & SGRIGNA, V. 2016. A regional adaptive and assimilative three-dimensional ionospheric model. *Advances in Space Research*, **57**, 10.1016/j.asr.2015.12.038.

SCOTTO, C. 2009. Electron density profile calculation technique for Autoscala ionogram analysis. *Advances in Space Research*, **44**, 10.1016/j.asr.2009.04.037.

SCOTTO, C. 2015. Triple splitting and z-rays in polar ionograms. *Antarctic Science*, **27**, 10.1017/S095410201400090X.

SCOTTO, C. & PEZZOPANE, M. 2002. A software for automatic scaling of *fo*F2 and *MUF*(*3000*)F2 from ionograms. *Proceedings of the 27th General Assembly of the International Union of Radio Science*. Ghent: International Union of Radio Science.

SCOTTO, C. & PEZZOPANE, M. 2012. Automatic scaling of polar ionograms. *Antarctic Science*, **24**, 10.1017/S0954102011000587.

SHIMAZAKI, T. 1962. A statistical study of occurrence probability of spread f at high latitudes. *Journal of Geophysical Research*, **67**, 10.1029/JZ067i012p04617.

SIDDLE, D.R., STOCKER, A.J. & WARRINGTON, E.M. 2004a. The time-of-flight and direction of arrival of HF radio signals received over a path along the mid-latitude trough: observations. *Radio Science*, **39**, 10.1029/2004RS003049.

SIDDLE, D.R., ZAALOV, N.Y., STOCKER, A.J. & WARRINGTON, E.M. 2004b. The time-of-flight and direction of arrival of HF radio signals received over a path along the mid-latitude trough: theoretical considerations. *Radio Science*, **39**, 10.1029/2004RS003052.

STANISLAWSKA, I. & ZBYSZYNSKI, Z. 2002. Forecasting of ionospheric characteristics during quiet and disturbed conditions. *Annals of Geophysics*, **45**, 169–175.

TESTUD, J. 1970. Gravity waves generated during magnetic substorms. *Journal of Atmospheric and Terrestrial Physics*, **32**, 10.1016/0021-9169(70)90137-6.

TITHERIDGE, J.E. 1993. Computer-controlled operation of the IPS-42 ionosonde. *Proceedings of Session G6 at the 24th General Assembly of the International Union of Radio Science*. Available at: http://www.sws.bom.gov.au/IPSHosted/INAG/uag-104/text/tither.html.

WARRINGTON, E.M., ROGERS, N.C. & JONES, T.B. 1997. Large HF bearing errors for propagation paths contained within the polar cap. *IEE Proceedings - Microwaves Antennas and Propagation*, **144**, 10.1049/ip-map:19971187.

ZOLESI, B., BELEHAKI, A., TSAGOURI, I. & CANDER, L.R. 2004. Real-time updating of the Simplified Ionospheric Regional Model for operational applications. *Radio Science*, **39**, 10.1029/2003RS002936.

ZUCCHERETTI, E., TUTONE, G., SCIACCA, U., BIANCHI, C. & AROKIASAMY, B.J. 2003. The new AIS-INGV digital ionosonde. *Annals of Geophysics*, **46**, 647–659.